Viscoelastic model based force control for soft tissue interaction and its application in physiological motion compensation

Pedro Moreira, Nabil Zemiti, Chao Liu, Philippe Poignet

Viscoelastic model based force control for soft tissue interaction and its application in physiological motion compensation

Pedro Moreira, Nabil Zemiti, Chao Liu, Phillipe Poignet

LIRMM, UMR 5506, CNRS-Université Montpellier 2, 161 Rue Ada, 34095 Montpellier Cedex 05, France

Abstract

Controlling the interaction between robots and living soft tissues has become an important issue as the number of robotic systems inside the operating room increases. Many researches have been done on force control to help surgeons during medical procedures, such as physiological motion compensation and tele-operation systems with haptic feedback. In order to increase the performance of such controllers, this work presents a novel force control scheme using Active Observer (AOB) based on a viscoelastic interaction model. The control scheme has shown to be stable through theoretical analysis and its performance was evaluated by *in-vitro* experiments. In order to evaluate how the force control scheme behaves under the presence of physiological motion, experiments considering breathing and beating heart disturbances are presented. The proposed control scheme presented a stable behavior in both static and moving environment. The viscoelastic AOB presented a compensation ratio of 87% for the breathing motion and 79% for the beating heart motion.

Keywords: Force control, soft tissue modeling, robotically-assisted surgery, physiological motion compensation, beating heart surgery.

1. Introduction

Medical robotics has become a very active research topic in the last decades. The number of robotic systems inside the operating room is increasing and the benefits of performing robotically-assisted surgery are numerous. Robotized surgery presents many advantages over conventional surgery, such as reduced patient trauma, additional degrees of freedom, physiological motion compensation and tele-operation [5].

In most robotically-assisted medical procedures, the robot or the tool guided by the robot needs to get in contact with several types of soft tissues. Due to the delicacy of those tissues, safety is a major concern. The recent advances in force sensing technologies tend to increase the use of force information in surgical robots. Force control algorithms can be a powerful tool to increase safety and can be used to cope with many important issues, such as physiological motion compensation, control tissue deformation and haptic feedback during tele-operation.

Using force control is possible to assure the correct interaction between the robotic tool and the tissue [7]. Recently, force controllers have been used in tele-operateded systems to control the slave robot [21]. Those systemss have in common a trade-off between stability and transparency, which is greatly affected by the force control design. Some classical force controllers consider the environment as an elastic material. However, soft tissues are usually viscoelastic, nonlinear and inhomogeneous [39]. In addition, breathing and beating heart motions may induce disturbances, which make the interaction between the robotic tool and the human tissues a complex task to be controlled. In this intricate scenario, stability, robustness and bandwidth are important aspects of force control for surrgical robots.

This work aims to present a model based force controller for tool-tissue interaction. First, the work presents a soft tissue modeling, comparing different soft tissue models and selecting the most appropriated one. The force control scheme is designed based on a viscoelastic tissue model and its stability and robustness are theoretcaly analyzed. Experiments with static and moving environments are performed to evaluate the controller performance.

2. Previous work

This section presents some of the most relevant works in the two main topics of this paper. Many researches have been done in soft tissue modeling and force control for medical applications. A state of the art of each topic is presented next.

2.1. Soft tissue models

Several soft tissue models have been already proposed. In [34], soft tissue models are arranged in groups according to the final target application. Those groups can be classified according to two major constraints for almost all models, which are deformation accuracy and computation time. Fig. 1 summarizes the different types of applications according to these constraints. In scientific analysis field,

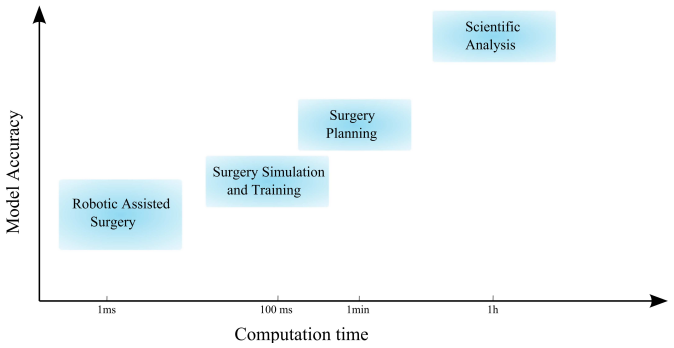

Figure 1: Relation between deformation accuracy and computation time for soft tissue models

the soft tissue model is used to validate physical hypothesis, to design new procedures or to diagnose a disease. In this case, the deformation accuracy is much more important than the computation time. In the surgery planning field, the computation time starts to become more relevant due to the need of several trials that must be performed. In the case of surgery simulation and training a smaller computation time is required to provide a smooth user interface. Finally, robotic assisted surgery requires real-time application, where deterministic computation time is of primary importance.

The models can also be divided in two main groups: analytical models and models based on Finite Element Method (FEM). FEM is a very widespread technique and is mostly used for tissue simulation. In FEM models, a tissue specimen is divided into a number of discrete elements forming a mesh [19]. The complete system may be complex and irregularly shaped, but the individual elements are easy to analyze. Despite its good accuracy, the applicability of FEM in real-time is still a challenge due the time necessary to compute the deformation of all individual element. Another issue of FEM based model is the influence of boundary conditions, which are very difficult to be defined *in-vivo* [18]. Analytical models can be developed to represent the interaction between robotic tools and soft tissues. These models can be broadly classified as linear elastic models, nonlinear elastic models and viscoelastic models [1].

Until today one of the most complete studies about the mechanical properties of soft tissue has been presented in [39]. In his book, Fung proposes a quasi-linear viscoelastic function to represent the stress-strain relationship. Unfortunately, Fung's model is very complex and has many parameters that must be estimated. In addition, as concluded by [28], small errors in the estimated parameters affect the simulation results. Another interesting model uses a combination of logarithmic functions and the Ogden model to describe the stress-strain relationship [26, 27]. However, the tests used to estimate the parameters are designed only for *in-vitro* tissues, which creates a drawback for its applicability on an intra-operative *in-vivo* situation. A model based on fractional derivatives is presented in [40]. Despite its good accuracy, the lack of recursiveness of fractional derivatives creates a drawback for using this model in real-time applications, limiting the use of this model to short real-time experiments.

The Hunt-Crossley is a popular model used to describe the impact of humanoid robots with soft environment [31]. This model has been used to represent soft tissues, such as presented by [25] and [29]. The model was first proposed by [30] in 1975 as a nonlinear model with viscous force proportional to the deformation depth.

In [33] a polynomial function of second order is proposed to model the interaction between the needle and the tissue during pre-puncture (e.g. surface contact). After the puncture the force is modeled by a sum of the cutting and friction forces. Other polynomial models can be defined, but higher order models have a large number of parameters to be estimated, which may compromise its applicability. In [29], palpation experiments on phantom tissues with polynomial models until 4^{th} order are presented. The results indicate that the accuracy between 2^{nd}, 3^{th} and 4^{th} order models are very close. The drawback of those polynomial models is the fact that they are adressed only to low frequency deformations.

A traditional way to represent viscoelastic materials is the combination between springs and dampers. These classical spring and damper models can also be used to represent soft tissue behavior [32]. They have the advantage of low computational cost and a physical meaning of each model parameter can be settled (i.e. springs represents the elasticity and dampers the viscosity). One of the goals of this work is to extend the analysis presented in [14] evaluating a comprehensive group of models and selecting the most suitable one for modeling the tool-tissue interaction during real-time applciations.

2.2. Force control in the medical robotics

One of the first works applying force control to medical robots is presented in [22], where the force feedback was used to provide safety, tactile capabilities and improve the man/machine interface. In this work, only rigid tissues were considered, since the main target was orthopedic surgeries. More recently, force control has been implemented on tool-tissue interaction, tele-operated systems with haptic feedback and also to reject disturbance forces caused by physiological motions.

In [6] a so called external force control is implemented in the Hippocrate Robot to control an ultrasound probe in contact with a human body. Latter, in [7], an external hybrid control is implemented in a skin harvesting robot. It consists of two embedded control loops combining position and force control. This architecture was developed to provide constant exerted force during the harvesting procedure. External force control schemes are well suited when simplicity, safety and implementation efficiency are of concern [6]. However, in the presence of physiological motion disturbances, bandwidth limitations can be an issue for such kind of controllers.

In [8], an impedance control is implemented in a hand held device to compensate disturbance motions. The presented results have shown that disturbance rejection was only possible with disturbances in a small range of low frequencies. In [3], a damping force control is implemented in a laparoscopic surgical robot without distal force sensing. Damping control is a particular implementation of impedance control [2], where the desired robot velocities are calculated based on the exerted force. However, in this work, the control performance is analyzed without considering physiological disturbances. Latter, in [37], a control loop based on Iterative Learning Control (ILC) is implemented in the same robot in addition to the conventional damping control loop. The ILC is used to compensate only for the breathing motions, based on the hypothesis that the disturbance is periodic.

In [38] a feedback force control based on Model Reference Adaptive Control is presented to compensate for beating heart motions. The control scheme uses the measures of the contact efforts applied by the robot on the heart surface and no *a priori* information about the beating heart motion is needed. The effectiveness and robustness of the proposed control are analyzed only through simulation results. However, the simulations presented do not consider noise in the force measures and as mentioned by [13], the noisy characteristic of force measurement is one of the major problems when performing force feedback control. A predictive force control based on a process model to predict future behavior using current and past forces is presented in [35]. A simulation study is introduced in [35] and experimental results using the proposed force controller are presented under beating heart disturbance motion in [36]. Despite the good results in simulation, the exhibited experimental results present a peak-to-peak force error of $2N$, wich means 20% of the applied force.

Clearly, the use of force control in the presence of complex physiological motions, especially when high frequencies are involved, is still a challenge. The force controllers previously proposed in the literature have in common the lack of a realistic soft tissue model. However, the influence of a more accurate tissue model in force controllers performance has been already proved [9, 14]. In order to safely perform robust and efficient force control under physiological motion disturbance, controllers with larger bandwidth and better stability parameters are needed. This work aims to the development of a force control based on soft tissue model to be used not only on static environments, but also in the presence of complex disturbance motions.

3. Soft tissue modeling

Understanding the interaction between medical tools and living tissues has become a very important aspect as the use of robot in medical application increases. Biomechanical characteristics of tissues are, in general, nonlinear, inhomogeneous and anisotropic [39]. These characteristics give the tissue a complex behavior when in contact with any kind of surgical instruments. Since the human body is mainly a complex combination of soft tissue, understanding and modeling these tissues are vital for the advancement of robotically-assisted surgery.

Model	**Equation**
Elastic	$f(t) = k \cdot x(t)$
K. Voigt	$f(t) = k \cdot x(t) + b \cdot \frac{x(t)}{dt}$
K. Boltzmann	$f(t) = \beta x(t) + \alpha \frac{x(t)}{dt} - \gamma \frac{f(t)}{dt}$
Maxwell	$f(t) = k \cdot x(t) + \alpha \cdot \frac{f(t)}{dt}$
Hunt-Crossley	$f(t) = k \cdot x^n(t) + \lambda \cdot x^n(t) \cdot \frac{x(t)}{dt}$
Fractional	$f(t) = G \frac{d^r x(t)}{dt^k}$

Table 1: Soft tissue candidate models

After a rigorous revision of the state of the art, it is necessary to define the most suitable model to be implemented in a real-time force controller. Therefore, a group of candidate models has been selected and evaluated under experiments, as it is described hereafter.

3.1. Soft tissue models for real-time application

It is almost a general consensus that no mathematical model can perfectly describe the complex behavior of soft tissues. But, it is possible to define a suitable model to be used in a control application as accurate as possible. Complex models such as the model based on the Ogden strain energy and the Quasi-linear model are excluded from our work due to their complexity and great number of parameters that must be estimated. Therefore, analyzing complexity and feasibility in real-time applications, six different models are chosen as candidate model:

1. Elastic model
2. Kelvin-Voigt model
3. Maxwell model
4. Kelvin-Boltzmann model
5. Hunt-Crossley model
6. Fractional model

Although the fractional model presents a lack of recursiveness in its calculation, we decided to include this model in the following off-line analysis due to its good results in recent publications [28]. A summary of the selected models can be seen on Table 1, where $f(t)$ is the exerted force and $x(t)$ is the tissue deformation. The elastic model is commonly used in robotic force control and is used in this work only as a reference for the comparison, since its limitation in representing the complex behavior of tool-tissue interaction is clear.

3.2. Experimental plan and setup

Several types of experiments can be performed in order to analyze the tissue behavior. Those experiments can be coarsely classified in two categories depending on the experimental conditions: experiments performed on a sample of tissue previously collected, called *in-vitro*, or performed directly on a living tissue, called *in-vivo*. It is clear that *in-vitro* specimens have limitations. Indeed, the biomechanical characteristics of an *in-vitro* specimen differ from the characteristics of living soft tissues. This fact can be explained mainly by the absence of vascularisation. On the other hand, performing a series of *in-vivo* experiments is quite complex and usually depends on the approval of one or more committees of ethics in clinical research. Nevertheless, the use of *in-vitro* specimen is very common and can provide results close to the one obtained with living tissues [39]. In the following subsections experiments with *in-vitro* conditions are presented to analyze and compare the soft tissue candidate models.

3.2.1. Experimental plan

The two most common experiments to analyze soft tissue behavior are relaxation and creep tests [39]. The relaxation test consists in performing a position step input (deformation) on the soft tissue surface and measuring the exerted force. The creep test is the opposite, a constant force is applied on the soft tissue and the deformation is measured. Other tests, such as a slow tissue compression presented in [24] can also be used to analyze the tissue behavior, but it catches the behavior of the tissue only at low frequencies. In [28] a special setup is presented to perform experiments to estimate the fractional model parameters. The experiments combine tissue compression and torsion, but the protocol was designed to be applied on *in-vitro* tissues only.

In this work, to identify the most suitable model, *in-vitro* relaxation tests are performed. Although the tests are performed *in-vitro*, it is important to notice that the proposed experimental protocol can be easily implemented and reproduced in an *in-vivo* clinical situation. The robot end-effector is positioned on the specimen surface, the robot moves in order to compress the tissue specimen with a position step. The robot motion and the exerted force are recorded and used in the evaluation process.

To evaluate each model, we divided the analysis in two subsections. In the first one, we estimate the unknown parameters and the exerted force using the same set of data. Two in-vitro spicimens are used and four relaxatin tests are perfored on each spicimen. The results are cmpared by a graphic inspectin to evaluate the symilarity of the dynamic behaviour of each model with the experimental results. The mean force estimatin error is also used to evaluate the accuracy of each model. After, the models are also compared in a cross-validation. The cross-validation is performed using the models defined by the average of the estimated parameters on four previous trials. The exerted forces are estimated using these average models under input data collected in a different trial.

Although one can argue about the excitation conditions to estimate the models parameters, the relaxation test is considered as a good way to estimate and analyze viscoelastic materials, as stated by [17]. In addition, all experiments presented in the following satisfy the condition for the estimation convergence.

3.2.2. Experimental setup

All tests are performed using the D2M2 robot. This robot has five degrees of freedom with direct drive technology providing potentially fast dynamics and low friction [4]. The first joint is prismatic and the other fours are revolute joints. The tool-tissue interaction forces are measured by a force sensor *ATI Mini40* (ATI Industrial Automation, Apex, USA) rigidly attached to the end effector. The tool in contact with the soft tissue is represented by a metallic cylinder with a diameter of $6mm$ (see Fig. 2b).

3.3. Estimation Technique

In order to estimate the model parameters, the linear least square method is used in the following subsections. The data (i.e. exerteded force and displacement) is collected in a series of relaxation tests and post-processed. The model parameters and the exerted force are offline estimated and compared. One can notice that the Hunt-Crossley model is a nonlinear model and for this reason, a different estimation technique should be used for this case. However, the results presented in [25] show that for a viscoelastic material the parameter n in the Hunt-Crossley model does not present a significant variation and is usually close to 1.3. In addition, using a large database of experiments and a nonlinear estimation technique, we could conclude that the parameter n has values around 1.26. To standardize the estimation, we consider in all cases $n = 1.26$, allowing the use of same estimation technique for all models (i.e. linear least square estimation). For the Fractional models, the derivative order is the same as presented by [15] ($r = 0.125$).

The general model equation is given by:

$$f = \theta_1\varphi_1(x) + \theta_2\varphi_2(x) + \cdots + \theta_n\varphi_n(x)$$

where, φ_1, φ_2, $\cdots$, φ_n are known functions, θ_1, θ_2, $\cdots$, θ_n are unknown parameters and f is the measured force, which has the property of being linear with respect to the parameters to be estimated. Therefore, the least square solution for this problem is given by [16]:

$$\hat{\theta} = (\Phi^t\Phi)^{-1}\Phi^t f \tag{1}$$

where,

$$\Phi = \begin{bmatrix} \varphi_1(x_1) & \varphi_2(x_1) & \cdots & \varphi_n(x_1) \\ \vdots & \vdots & \vdots & \vdots \\ \varphi_1(x_n) & \varphi_2(x_n) & \cdots & \varphi_n(x_n) \end{bmatrix}$$

We can guarantee that the least square problem has a solution given by (1) if $\Phi^t\Phi$ is non-singular. The matrix $\Phi^t\Phi$ will be non-singular if conditions are imposed on the input signal (sufficient richness or persistent). In the general least square problem, the estimation convergence is guaranteed if:

$$rank(\Phi) = dim(\theta) \tag{2}$$

In all tests that are presented in this paper, the convergence condition is guaranteed.

3.4. Experimental Results

Several relaxation tests are performed on two different soft tissue specimens. The first specimen is a pig's heart (Figure 2a) and the second one is a piece of beef (Figure 2b). The force estimation resuls and the cross-validatin results are presented next.

3.4.1. Parameters and force estimation

In this first group of experiments, the parameters for each model are estimated off-line and the estimated forces are compared to the measured force. Figure 3a shows the estimated and measured forces of one relaxation test performed on the pig's heart with a step input of $10mm$, Figure 3b shows the results of one relaxation test performed on the piece of beef with a step input of $8mm$. The average mean force estimation error for each model is presented in Table2. Analyzing the results presented in Table2, we can clearly see that the Kelvin Boltzmann, the Hunt Crossley and the Fractional models gave, among all models, the lowest estimation errors. Despite the slight poor accuracy of the Fractional model in the transient period observed by the graphic inspection, its relaxation accuracy had influenced the mean estimatin error.

As expected, looking at Figure 3a, we can see that the elastic model reaches approximately the final value, but it does not follow the tissue dynamics. The Kelvin-Boltzmann model and the Hunt-Crossley model have the most realistic response, reaching approximately the final value and following the tissue dynamic. The Kelvin-Voigt model also presents a behavior similar to the tissue dynamic, but less accurate if compared with the previous

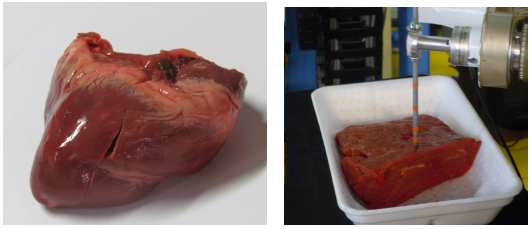

(a) (b)

Figure 2: *In-vitro* specimens used in relaxation tests: (a) Pig's heart; (b) Beef

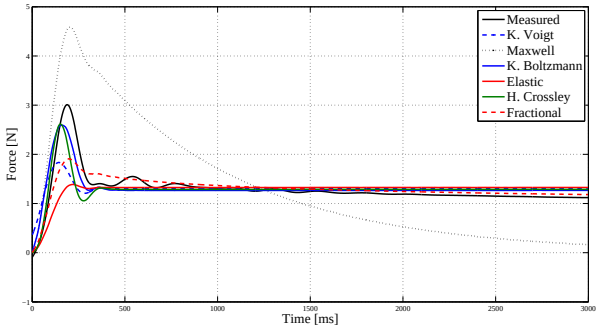

(a)

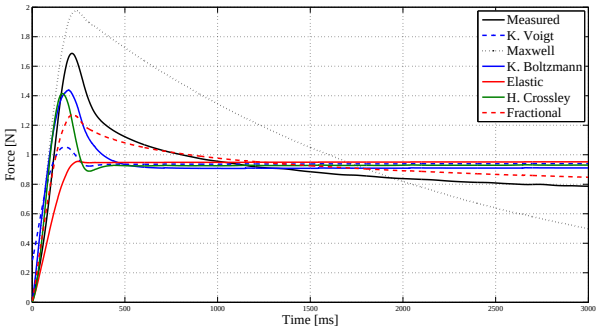

(b)

Figure 3: Measured and estimated forces relaxation tests: (a) performed on the pig's heart (b) performed on the beef

two models. The Fractional model presents a good force estimation only after the transient period.

The same conclusion can be reached analyzing Figure 3b. While the Kelvin Boltzmann and the Hunt-Crossley model gave the best transient estimation, the Fractional model presents a good estimation after the transient (i.e. relaxation period). As concluded in [12], the Fractional model can be a very accurate model under slow or static deformations. On the other hand, when fast deformations are applied, the Fractional model may not represent the tissue behavior as accurate as the Kelvin Boltzmann or the Hunt-Crossley models.

3.4.2. Cross validation

The cross-validation is important to mathematically approximate tissue dynamic behavior, since we aim to model real tissues, which are inhomogeneous [24]. Analyzing the models under the cross-validation, we can evaluate how a previously identified model predicts the force using a new set of data.

For the cross-validation, each model is defined using the average of the parameters estimated in four relaxation tests. Two cross-validation are presented, one using the database collected in experiments performed on the pig's heart and the other using the database collected on experiments performed on the beef.

Model	Mean force estimation error (N)
Elastic	0.124 ± 0.038
K. Voigt	0.449 ± 0.229
K. Boltzmann	0.115 ± 0.038
Maxwell	0.092 ± 0.031
Hunt-Crossley	0.091 ± 0.030
Fractional	0.065 ± 0.019

Table 2: Average of mean force estimatin error and standard deviation

The estimated forces in the cross-validation using the heart database (step input of $10mm$) can be seen in Figure 4a. The results using the beef database are presented in Figure 4b (step input of $8mm$).

3.5. Analysis

Among the six candidate models, the Kelvin-Boltzmann, the Hunt-Crossley and the Fractional models have shown the best results. The Kelvin Boltzmann and the Hunt-Crossley stood out specially in the transient response, while the Fractional model showed a good estimation during the relaxation period.

Although the Fractional model gave a good force estimation during the relaxation time, its poor accuracy in the transient period and the lack of recursiveness to calculate the fractional derivatives are major drawbacks to use this model within a model based force control scheme.

By graphic inspection, it is clear that the Kelvin Boltzmann and the Hunt-Crossley models gave the best results in terms of both transient performance and accuracy. However, the Hunt-Crossley and the Kelvin Boltzmann models have significant differences. While the Kelvin Boltzmann model is a linear model, the Hunt-Crossley is nonlinear. The Kelvin Boltzmann linearity is an advantage of using it within a model based force controller, mainly because of the possibility to use standard techniques to analyze linear systems. In addition, in the Kelvin Boltzmann model the elastic force is given by the term $\beta x(t)$. Thus, we can define the parameter β as the purely elastic parameter (i.e. stiffness). This stiffness parameter definition is important to analyze the static error presented in the cross-validation. During the relaxation period, $\dot{x}(t)$ is zero and $\dot{f}(t)$ has very low values, for this reason, this static error can be imputed to a mismatch on the stiffness parameter. This mismatch is explained due to the tissue inhomogeneity, which gives a different stiffness depending on the contact point where the experiment is performed. One solution for this problem is to implement an on-line estimation of the stiffness parameter. Moreover, this on-line estimation allows the proposed model based force control to be directly applicable on *in-vivo* tissues, dealing with tissue inhomogeneities.

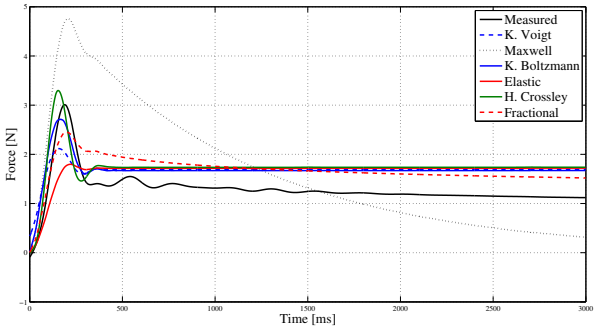

(a)

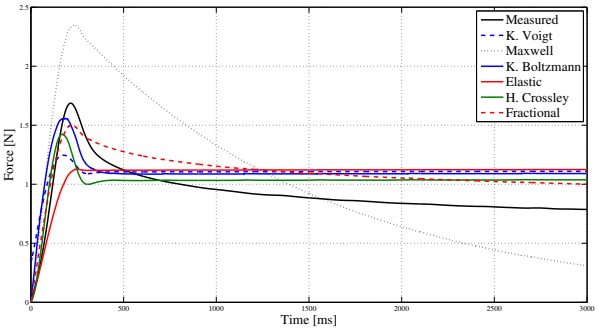

(b)

Figure 4: Cross validation in relaxation tests: (a) using pig's heart database (b) using beef database

In conclusion, because of its good accuracy and transient performance, its physical meaning, and linear properties, the Kelvin Boltzmann is defined as the best model to be inserted within the model based force control.

4. Model based force control

In this section the force control architecture based on the chosen soft tissue model is presented. The proposed control scheme is a state space feedback using Active Observer (AOB). The AOB is a stochastic observer used to estimate the system states and an extra state, which is added to compensate for modeling errors and system disturbances [41]. In this section the system design and its stability and robustness analysis are presented.

4.1. Robot and environment modeling

Considering a robot with n degrees of freedom and joint coordinates q, the free space motion in the joint space can be written in the form [42]:

$$M(q)\ddot{q} + V(q,\dot{q}) + G(q) = \tau_c, \tag{3}$$

where $M(q)$ is the robot inertial matrix, $V(q,\dot{q})$ represents the Coriolis and centrifugal forces, $G(q)$ is the gravity forces matrix and τ is the generalized forces in joint space. Equation (3) can be rewritten using the Cartesian space formulation

$$M_x(q)\ddot{X} + V_x(q,\dot{q}) + G_x(q) = F_c \tag{4}$$

The vector X is the Cartesian coordinates and the relationship between Cartesian and angular velocities is given by:

$$\dot{X} = J(q)\dot{q} \tag{5}$$

The relationship between the generalized end-effector forces F_c and the generalized joint space forces is given by:

$$\tau_c = J^t(q)F_c \tag{6}$$

The matrix $J(q)$ is the Jacobian matrix and $J^t(q)$ is the transposed Jacobian matrix. The inertial, the gravity and the Coriolis and centrifugal Cartesian matrices are given by [10]:

$$\begin{aligned} M_x(q) &= J^{-t}M(q)J^{-1} \\ V_x(q,\dot{q}) &= J^{-t}V(q,\dot{q}) - M_x(q)\dot{J}(q)\dot{q} \\ G_x(q) &= J^{-t}G(q) \end{aligned}$$

In addition, when the robot is in contact with an environment, a new force component appears in the dynamic equation due to this contact. Thus, including the exerted force F_e in (4) we obtain:

$$M_x(q)\ddot{X} + V_x(q,\dot{q}) + G_x(q) = F_c - F_e, \tag{7}$$

where the vector F_e is composed by the force exerted in each Cartesian axis (f_e). Considering $\hat{M}_x(q)$, $\hat{V}_x(q,\dot{q})$ and $\hat{G}(q)$ the estimations of $M_x(q)$, $V_x(q,\dot{q})$ and $G(q)$, we can design a control law given by:

$$F_c = \hat{M}_x(q)U + \hat{V}_x(q,\dot{q}) + \hat{G}(q) + \hat{F}_e \tag{8}$$

Substituting (8) in (7), it is possible to achieve a decoupled second order system along each Cartesian axis such as

$$U = \ddot{X} \tag{9}$$

The vector U is composed by the control signals for each degree of freedom. This linearization allows us to transform a complex nonlinear problem given by (7) into a simple linear decoupled problem given by (9). The decoupled characteristics of the linearized system allows us to control each degree of freedom independently (position and orientation). In this work, since we are dealing with a ponctual contact point, we focus on the control of the robot Cartesian position.

To improve stability and robustness under modeling errors, an inner velocity loop with a diagonal matrix gain

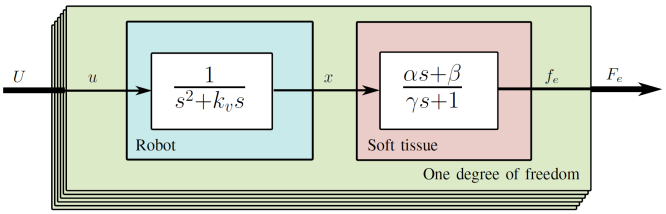

Figure 5: Open loop system considering the linearized robot and the Kelvin Boltzmann model in frequency domain, where s is the Laplace operator. The input is the contrl signal u and the output is the exerted force f_e.

K_v is added in the system. The differential equation is then given by:

$$U = \ddot{X} + K_v\dot{X} \tag{10}$$

The differential equation (10) relates the input U with robot end-effector coordinates given by X. The system is fully decoupled and each degree of freed, i.e., each Cartesian axis, can be independently writen as

$$u = \ddot{x} + k_v\dot{x} \tag{11}$$

where $\dot{x}$ and $\ddot{x}$ are ne degree f freedom velocity and acceleration, and u is the control input. We can introduce the environment model (e.g. the soft tissue model) in the differential equation (10) to relate the control input to the exerted force, as depicted in Figure 5. Since the system is decoupled, the control design is done for one degree of freedom and can be easily replicated to the other degrees of freedom. Using the Kelvin Boltzmann model, the differential equation for each Cartesian axis can be written as

$$(\alpha/\gamma)\dot{u} + (\beta/\gamma)u = \dddot{f}_e + (k_v + 1/\gamma)\ddot{f}_e + (k_v/\gamma)\dot{f}_e \tag{12}$$

where α, β and γ are the Kelvin Boltzmann parameters and f_e is the exerted force in one Cartesian axis. The transfer function in frequency domain describing the relation between the input u and the force output f_e is given by

$$G(s) = \frac{(\alpha/\gamma)s + (\beta/\gamma)}{s^3 + (k_v + 1/\gamma)s^2 + (k_v/\gamma)s} \tag{13}$$

where s is the Laplace operator.

The system (13) can also be represented in state space form. There are several ways to find a state space representation of a system. Aiming a state space equation to be used in a control scheme with a state observer, the Observable Canonical Form (OCF) realization is chosen [23]. Then, from (13), the OCF realization is obtained in a straightforward way

$$\begin{bmatrix} \dot{x_1} \\ \dot{x_2} \\ \dot{x_3} \end{bmatrix} = \begin{bmatrix} -k_v - 1/\gamma & 1 & 0 \\ -k_v/\gamma & 0 & 1 \\ 0 & 0 & 0 \end{bmatrix} \begin{bmatrix} x_1 \\ x_2 \\ x_3 \end{bmatrix} + \begin{bmatrix} 0 \\ \alpha/\gamma \\ \beta/\gamma \end{bmatrix} u(t) \tag{14}$$

$$f(t) = \begin{bmatrix} 1 & 0 & 0 \end{bmatrix} \begin{bmatrix} x_1 \\ x_2 \\ x_3 \end{bmatrix} = Cx \tag{15}$$

Considering that the system is preceded by a zero order hold (ZOH), the stochastic discrete state space representation is given by:

$$\begin{cases} x_k = \Phi x_{k-1} + \Gamma u_{k-1} + \xi_k \\ y_k = C x_k + \eta_k \end{cases} \tag{16}$$

where Φ is the discrete state matrix and Γ is the discrete input matrix. These matrix can be easily obtained from (14) [16]. With a known state space representation, one can, now, define the pole placement control law. The control law is commonly defined as the feedback of a linear combination of all states elements, such as:

$$u = -Lx + r \tag{17}$$

where L is the state feedback gain and r is the force reference input. The Ackermann's formula is used to calculate the feedback gain L.

4.2. Viscoelastic Active Observer

The goal of a classical observer is to estimate the system states based on the system equations and measurements. In a perfect scenario, the estimated states $\hat{x}_k$ should be a copy of the system states x_k. However, in practical application, one cannot guarantee that $\hat{x}_k = x_k$. An estimation error e_k is always associated to the state estimation, such as:

$$\hat{x}_k = x_k - e_k \tag{18}$$

When a state feedback is performed using an observer, the estimation error e_k enters in the system as an additional undesired input. Using the AOB, an extra state is added to estimate this error and to compensate it using the so called active state, given by:

$$p_k = Le_k \tag{19}$$

The AOB scheme is depicted in Figure 6, the active state estimation $\hat{p}_k$ appears in the feedback loop to cancel the effect of the state estimation error.

According to [41], a deterministic approach to model the active state p_k has many limitations, for this reason a stochastic approach is used, given to the p_k the following evolution equation:

$$p_k - p_{k-1} = \omega_k \tag{20}$$

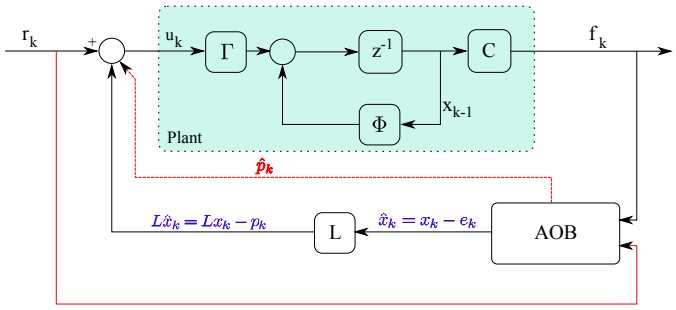

Figure 6: Active observer diagram: the active state estimation $\hat{p}_k$ tries to compensate p_k

in which ω_k is a zero-mean Gaussian random variable. It is important to notice that ω_k is seen by the Kalman equation used in the AOB algorithm as a white noise. Although, it describes the evolution of p_k [20].

Introducing the active state in the system equation (16), we have:

$$\begin{cases} \begin{bmatrix} x_k \\ p_k \end{bmatrix} = \begin{bmatrix} \Phi & \Gamma \\ 0 & 1 \end{bmatrix} \begin{bmatrix} x_{k-1} \\ p_{k-1} \end{bmatrix} + \begin{bmatrix} \Gamma \\ 0 \end{bmatrix} u'_{k-1} + \begin{bmatrix} \xi_{x_k} \\ \omega_k \end{bmatrix} \\ y_k = C_a \begin{bmatrix} x_k \\ p_k \end{bmatrix} + \eta_k \end{cases} \tag{21}$$

with

$$u'_{k-1} = r_{k-1} - \begin{bmatrix} L & 1 \end{bmatrix} \begin{bmatrix} x_{k-1} \\ \hat{p}_{k-1} \end{bmatrix}$$

and

$$C_a = \begin{bmatrix} C & 0 \end{bmatrix}$$

The desired closed loop system appears when $\hat{p}_k = p_k$:

$$\begin{bmatrix} x_k \\ p_k \end{bmatrix} = \begin{bmatrix} \Phi - \Gamma L & 0 \\ 0 & 1 \end{bmatrix} \begin{bmatrix} x_{k-1} \\ p_{k-1} \end{bmatrix} + \begin{bmatrix} \Gamma \\ 0 \end{bmatrix} r_{k-1} + \begin{bmatrix} \xi_{x_k} \\ \omega_k \end{bmatrix} \tag{22}$$

The state estimation is based on (22) and it is given by:

$$\begin{bmatrix} \hat{x}_k \\ \hat{p}_k \end{bmatrix} = \begin{bmatrix} \Phi - \Gamma L & 0 \\ 0 & 1 \end{bmatrix} \begin{bmatrix} \hat{x}_{k-1} \\ \hat{p}_{k-1} \end{bmatrix} + \begin{bmatrix} \Gamma \\ 0 \end{bmatrix} r_{k-1} + K_k(y_k - \hat{y}_k) \tag{23}$$

where,

$$\hat{y}_k = C_a \left(\begin{bmatrix} \Phi - \Gamma L & 0 \\ 0 & 1 \end{bmatrix} \begin{bmatrix} \hat{x}_{k-1} \\ \hat{p}_{k-1} \end{bmatrix} + \begin{bmatrix} \Gamma \\ 0 \end{bmatrix} r_{k-1} \right) \tag{24}$$

The matrix K_k is the Kalman gain and is related to the uncertainty of each state. The Kalman gain is calculated by:

$$K_k = P_{1k} C_a^T (C_a P_{1k} C_a^T + R_k)^{-1}$$

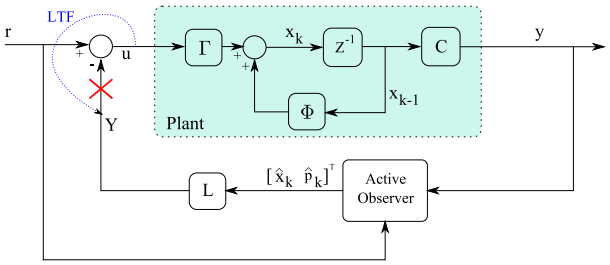

Figure 7: Schematic diagram for the loop transfer function (LTF)

$$P_{1k} = \Phi_a P_{k-1} \Phi_a^T + Q_k$$

$$P_k = P_{1k} - K_k C_a P_{1k}$$

The matrix Φ_a is called the augmented open loop matrix and has the form:

$$\Phi_a = \begin{bmatrix} \Phi_r & L_r \\ 0 & 1 \end{bmatrix}$$

The matrix Q_k is the system covariance noise and R_k is a scalar value related to the measurement covariance noise. Q_k has the form:

$$Q_k = \begin{bmatrix} Q_x & 0 \\ 0 & Q_p \end{bmatrix}$$

The estimation strategy depends on the relation between Q_k and R_k values. If the model accuracy is higher than the measurement accuracy ($Q_k << R_k$), a model-based approach (MBA) is considered with low Kalman gain values. On the other hand, if the measurement is more accurate ($Q_k >> R_k$), a sensor based approach (SBA) is followed with high Kalman gain values. Another important aspect in the AOB tuning is the relation between Q_x and Q_p, the higher the value of Q_p is with respect to Q_x, the more active the extra state will be.

4.2.1. System stability

Phase and gain margins are the most common indicators to analyze relative stability. In the case of systems with observers, this analysis can be made through the loop transfer function (LTF). Figure 7 presents the schematic representation of LTF for a system with observer, where r is the system input and y the system output. The LTF is then the relation between the control input u and the LTF output Y.

The corresponding LTF for proposed force controller is given by:

Rise time [s]	Phase Margin	Gain Margin
0.980	87.53°	7.66
0.600	84.29°	5.92
0.225	57.40°	4.13
0.090	30.73°	3.42

Table 3: Phase and gain margins with different desired rise times ($Q_x = 10^{-7}$, $Q_p = 10^{-4}$, $R_k = 10^{-3}$)

$$\begin{cases} \begin{bmatrix} \hat{x}_k \\ e_k \end{bmatrix} = \begin{bmatrix} \Phi - (I - K_k C)\Gamma L & K_k C \Phi \\ (I - K_k C)\Gamma L & (I - K_k C)\Phi \end{bmatrix} \cdot \begin{bmatrix} \hat{x}_{k-1} \\ e_{k-1} \end{bmatrix} + \\ \qquad + \begin{bmatrix} K_k C \Gamma \\ (I - K_k C)\Gamma \end{bmatrix} u_{k-1} \\ Y = \begin{bmatrix} L & 0 \end{bmatrix} \cdot \begin{bmatrix} \hat{x}_k \\ e_k \end{bmatrix} \end{cases} \tag{25}$$

For the following analysis, the Kelvin Boltzmann tissue model identified in the last section is used, The model is given by the equation:

$$f(t) = 190x(t) + 27\frac{dx(t)}{dt} + 0.0345\frac{df(t)}{dt} \tag{26}$$

The AOB is conservatively tuned to have a model based behaviour with the values:

$$Q_x = 10^{-7},\ Q_p = 10^{-4},\ R_k = 10^{-3}$$

Four different desired closed loop behaviors are selected to have its relative stability analyzed. The closed loop behavior is given by the desired rise time and it is set to have no overshoot. The desired rise times are chosen between a very slow time response (0.980 seconds) and a fast time response (0.090 seconds). Table 3 presents the phase and the gain margins for four different desired closed loop behavior. One can conclude that a trade-off between rise time and stability appears in the control design.

The AOB tuning is also determinant to the system stability.The tuning is done by selecting the values of Q_x, Q_p and R_k. The relation between Q_x and Q_p gives how adaptive is the AOB, and the relation between Q_x and R_k determines if the system has a model based approach (MBA) or a sensor based approach (SBA). Three AOB tunings are selected to analyze their phase and gain margins: in the first two cases the AOB is set as model based (i.e. $Q_x < R_k$). In the third case $Q_x = R_k$, which means the AOB is set with a sensor based approach (SBA). The rise time chosen for all cases is an intermediate value among the values listed in Table 3: $0.600s$.

The results presented in Table 4 shows that increasing Q_x the AOB reduce its stability margins. As we increase the value of Q_x, the active state increases its capability of compensating for modeling errors, but on the other hand we decrease phase and gain margins. Although the SBA may present a better error compensation, it can be undesired in a real application due to the proximity to instability. At this point one can find a trade off between modeling error compensation and stability.

	Tuning	Phase Margin	Gain Margin
Case 1 (MBA)	$Q_x = 10^{-7}$	84.29°	5.92
Case 2 (MBA)	$Q_x = 10^{-5}$	79.94°	8.92
Case 3 (SBA)	$Q_x = 10^{-3}$	41.41°	20.26

Table 4: Phase and gain margins with different AOB tunings and desired rise time of 0.600s. The values of Q_p and R_k in the three cases are 10^{-4} and 10^{-3} respectively.

4.2.2. System Robustness

The robustness analysis is performed to understand how parameter mismatches affect the system stability. The goal of this subsection is to define, in theory how much errors the system can handle and which parameter is more sensitive to errors.The robustness analysis is done through the relative stability when parameter mismatches occur. For a given parameter error, the AOB matrices have to be calculated such as:

$$\Phi_n = \Phi - \Delta\Phi \tag{27}$$

$$\Gamma_n = \Gamma - \Delta\Gamma \tag{28}$$

where, Φ_n and Γ_n are the nominal matrices used in the AOB design and $\Delta\Phi$ and $\Delta\Gamma$ are the errors induced by the parameter mismatches. Then, the relative stability is obtained by the LTF given by:

$$\begin{cases} \begin{bmatrix} \hat{x}_k \\ e_k \end{bmatrix} = \begin{bmatrix} \Phi_n - \Gamma_n L + K_k C(\Delta\Phi + \Gamma_n L) & K_k C\Phi \\ (I - K_k C)(\Delta\Phi + \Gamma_n L) & (I - K_k C)\Phi \end{bmatrix} \cdot \\ \qquad \cdot \begin{bmatrix} \hat{x}_{k-1} \\ e_{k-1} \end{bmatrix} + \begin{bmatrix} K_k C\Gamma \\ (I - K_k C)\Gamma \end{bmatrix} \\ Y = \begin{bmatrix} L & 0 \end{bmatrix} \cdot \begin{bmatrix} \hat{x}_k \\ e_k \end{bmatrix} \end{cases} \tag{29}$$

In the Kelvin Boltzmann model, the mismatch can occur on three parameters. To study the influence of the mismatch in the parameters, an error has been added on each parameter separately and also on the three parameters at the same time. Four cases have been considered, such as:

1. Case (a): $\alpha_r = \delta \cdot \alpha$, $\beta_r = \beta$ and $\gamma_r = \gamma$
2. Case (b): $\alpha_r = \alpha$, $\beta_r = \delta \cdot \beta$ and $\gamma_r = \gamma$
3. Case (c): $\alpha_r = \alpha$, $\beta_r = \beta$ and $\gamma_r = \delta \cdot \gamma$
4. Case (d): $\alpha_r = \delta \cdot \alpha$, $\beta_r = \delta \cdot \beta$ and $\gamma_r = \delta \cdot \gamma$

with $\{\delta \in \mathbb{R} \| 0.8 \leq \delta \leq 4.0\}$. It means that in case (a) the error is added only on α, in case (b) the error is added only on β, in case (c) the error is added only on γ and in the last case the error is added on all three parameters simultaneously.

Of course this analysis is quite simplistic, since in a real situation it is unusual to get a linear parameter mismatch. In fact, the definition of how this mismatch occurs on a soft tissue is almost impossible due to the inhomogeneity presents on soft tissues. However, this analysis helps to understand how those mismatches affect the system stability. The soft tissue model used is the same as the one presented in the last subsections and the AOB is tuned as a model based with:

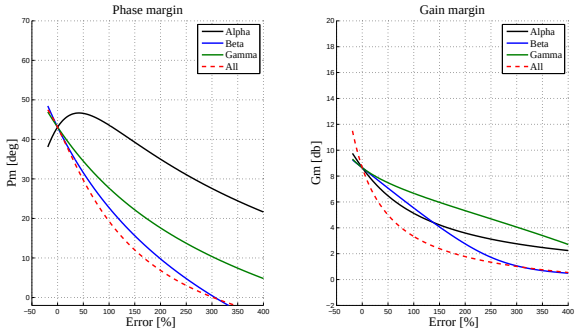

Figure 8: Phase and gain margins with parameter mismatches

$$Q_x = 10^{-5},\ Q_p = 10^{-4},\ R = 10^{-3}$$

Using (29), the phase and gain margins are calculated. The curves of phase and gain margins versus the parameter errors in percentage are shown in Figure 8.

The phase margin analysis shows that, the system has proved to be stable with real parameter values up to 300% ($Pm = 0$) higher than the nominal parameters. It is possible to observe that for all analyzed cases, the system becomes unstable as the mismatch becomes larger. Anyhow, looking at the graph one can conclude that the mismatches in α and γ change the phase and gain margins, but do not create unstable systems. On the other hand, the stiffness parameter β can be pointed as the critical parameter, unstabilizing the system when the mismatch approaches 300%. It is also the one that mostly determines the phase margin when errors are presented in all parameters. To cope with this mismatch problem an on-line estimation of the stiffness parameter is included in the system during the experiments.

5. Experimental Results

In this section, the experimental results are presented. In order to evaluate the proposed force control, experiments with surface contact on a static environment and on a moving environment are performed. The static experiment is performed on an in-vitro tissue and the moving environment experiments are performed on a polyvinyl chloride (PVC) phantom. The PVC phantom was used because it has been used in previous works to represent human soft tissue due to its properties similar to human tissues [43, 44, 45]. The moving environment is created to simulate physiological motions. In addition, to increase the system robustness an on-line estimation of the stiffness parameter is performed.

5.1. On-line parameter estimation

The model parameters may vary due to the complexity of tissues and its inhomogeneity. For that reason, an on-line updating of parameters is desirable and can increase the relative stability of the system. In theory, the three parameters of the Kelvin Boltzmann model can be estimated, but in practice we can only guarantee convergence in the estimation of parameters when it is sufficiently excited. For instance when the interaction between the robot and the tissue is smooth, the tissue viscosity may not be excited enogth, leading to false estimated values of α and γ. Additionally, according to the results given in section 4.2.2, the mismatch in the parameter β is the one that most influences the stability of the system. Therefore, we decided to perform an on-line estimation on the parameter β.

The parameters α and γ are estimated off-line as described in Section 3 and will not be updated. However, since the off-line estimation protocol is adaptable to *in-vivo* situations, pre-operative tests can be perform to estimate these two parameters in an *in-vivo* clinical scenario. Therefore, the Kelvin Boltzmann model is written as:

$$f(t) = -\alpha\frac{df(t)}{dt} + \gamma\frac{dx(t)}{dt} + \beta_k x(t)$$

where β_k is the stiffness parameter estimated on-line by a Kalman Filter. The estimation of β is used to update the AOB matrices and the feedback gain matrix.

5.2. Static environment

For this experiment the AOB is tuned as MBA, with $R = 0.01$, $Q_x = 10^{-9}$ and $Q_p = 10^{-5}$. The off-line estimated parameters for the *in-vitro* specimen are:

- $\alpha = 34.3$, $\beta = 200.0$ and $\gamma = 0.024$.

The desired closed loop poles are allocated together in $s = -10$, given a closed loop behavior with no overshoot and a rise time of $213ms$. The initial feedback matrix is:

$$L = \begin{bmatrix} 0.809 & -0.019 & 0.00076 \end{bmatrix}$$

The measured force as well as the desired force and the estimated force are plotted in Figure 9. The on-line estimation of the stiffness parameter β, shown in Figure 10, illustrates how the soft tissue stiffness changes during the experiment. The experimental result shows a satisfactory behavior, following the desired trajectory without neither overshoot nor static error.

5.3. Moving environment

The motion compensation experiments are performed using two robots (Figure 11). The force control algorithm is implemented in the D2M2 robot. The second robot is a Viper S650, which holds a phantom made of polyvinyl chloride (PVC) and performs the disturbance motion. The Viper controller is running a position control with sampling frequency of $1kHz$ and is set to perform breathing motion or beating heart motion. It is important to notice that the D2M2 robot has no previous information about the disturbance motion performed by the Viper robot. Figure 11 shows the experimental platform used in the following experiments. The tissue used in the next experiments is a PVC phantom with the following Kelvin Boltzmann parameters:

$$\alpha = 5.0,\ \beta = 290.0 \text{ and } \gamma = 0.02.$$

The AOB is tuned with $Q_x = 10^{-11}$, $Q_p = 10^{-6}$, $R_k = 10^{-2}$. The desired closed loop is set to give no overshoot and rise time of $0.080s$. Ideally, higher values of Q_p should give better compensation results. However, it was not possible to experimentally tune the AOB with higher values of Q_p without compromising the stability of the system.

5.3.1. Breathing motion

For the breathing motion experiment, the disturbance is given by a sinusoidal wave with $0.2Hz$ of frequency and $5mm$ of amplitude.

Figure 12 shows the force measurements during the experiments with breathing motion disturbance with and without force control. When the force control is off, the peak force error has amplitude around $0.9N$,which means 45% of the desired force. When the force control is running, the peak-to-peak force error is reduced to $0.1N$, which means 5% of the desired force. The control input and the active state estimation can be seen in Figure 13. It is possible to observe that the active state has an important role in the control input. This happens because it compensates not only for the modeling errors, but also for the disturbance motion.

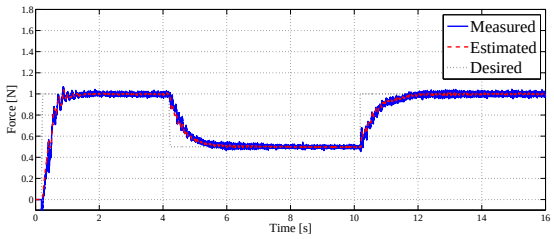

Figure 9: Force information during experiments on pig's heart surface

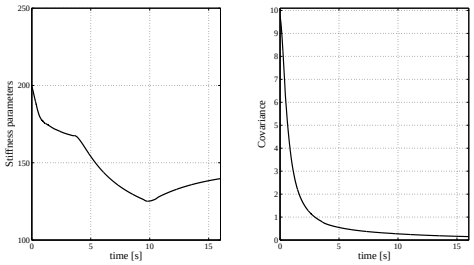

Figure 10: Parameter estimation and its covariance during experiments on specimen 2

Figure 11: Experimental platform for motion compensation: The D2M2 robot is running the force control and the Viper Robot performs the disturbance motion. The force control is used to keep the contact force constant even in the presence of disturbances.

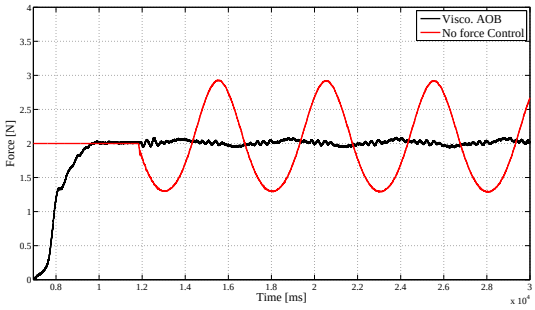

Figure 12: Force measurements with breathing disturbance motion: the red line is the measured force with no force control and the black line is the measured force when the proposed force control is running. The desired exerted force is 2N

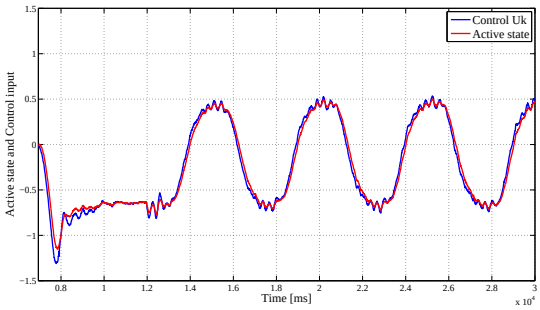

Figure 13: Control input and active state during breathing motion compensation

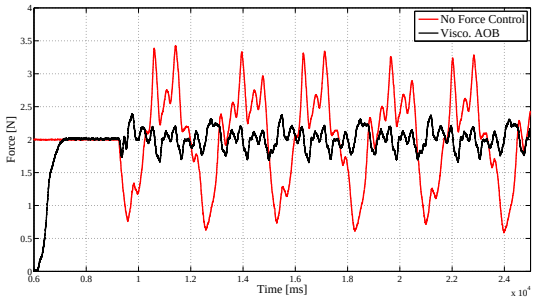

Figure 14: Force measurements with beating heart disturbance motion: the red line is the measured force with no force control and the black line is the measured force when the proposed force control is running. The desired exerted force is 2N

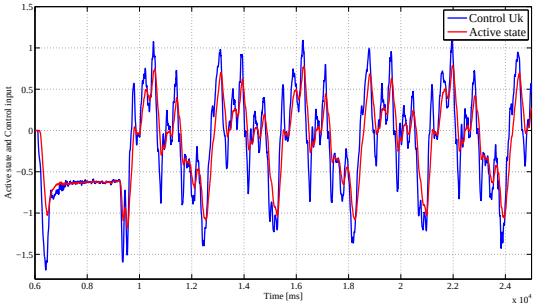

Figure 15: Control input and active state during beating heart motion compensation

5.3.2. Beating heart motion

For the beating heart motion experiment, the disturbance is given by the heart motion recorded *in-vivo* by a Da Vinci System (Intuitive Surgical Inc., Sunnyvale, USA) [11]. The motion in Z axis is chosen due its complexity, including breathing and heart motion and also having the larger amplitude of all axis.

Figure 14 shows the force measurements during the experiments with beating heart motion disturbance. When the force control is off, the peak force error has amplitude around $1.4N$,which means 70% of the desired force. When the force control is running, the force error is reduced to $0.3N$, which means 15% of the desired force. The control input and the active state estimation can be seen in Figure 15.

5.4. Discussion

The presented experiments have shown that the proposed model based force control presents a stable behavior even in the presence of disturbance motions. On the static environment, the controller has presented a performance with no overshoot and no static error. In addition, the on-line estimation of β has proved its ability to deal with

inhomogeneities and nonlinearities present on the tissue stiffness.

On the moving environment, the controller was able to compensate for complex physiological motions used as disturbance. The effectiveness of motion compensation can be evaluated by the compensation ratio (i.e the relation between the peak-to-peak force error with and without force control). For breathing disturbance motion, the system had a compensation ratio of 87%. A compensation ratio of 79% is achieved when the beat heart motion is applied as disturbance. Unfortunatelly, there are just a few works dealing with beating heart motion compensation using force control under experimental results, but comparing our results with a previous work, a compensation ratio for beating heart motion of 72% is presented in [36].

The theory shows that the viscoelastic AOB could achieve an even better disturbance rejection if a more aggressive tuning is performed. However, many characteristics of the experimental setup influence the AOB tuning. One important issue is the presence of noise on the force measurements. Therefore, the motion compensation can be improved by using a force sensor with higher signal-to-noise ratio.

6. Conclusion

This paper has presented a model based force control for tool-tissue interaction. In this context, a soft tissue model was selected among several candidate models. The Kelvin Boltzmann model was chosen due to its accuracy and feasible of implementation. This model was introduced in a force control scheme. The preliminary results presented in [14] have already shown by experiments how a viscoelastic model can improve a force control scheme for tool-tissue interaction. In this paper, the stability and robustness of the control scheme were also theoretically evaluated. The force control was also evaluated under moving environments and its ability of compensating physiological motions was analyzed. The results have shown that a compensation ratio of 87% was achieved for breathing motion. Regarding the beating heart motion, the compensation ratio of 79% was obtained.

Further work will focus on the on-line estimation of all soft tissue parameters and its convergence. We are also focus on implementing this control scheme for motion compensation in tele-operated systems, which is already undergoing. Experiments on *in-vivo* situation are also planned.

Conflict of interest

There is not conflict of interest.

Acknowledgement

This work was granted by ANR Contint USComp project

Bibliography

[1] S. Misra, K. T. Ramesh, A. M. Okamura, Modeling of tool-tissue interactions for computer-based surgical simulation: a literature review, Presence: Teleoperators and Virtual Environments 17 (5) (2008) 463–491.

[2] N. Zemiti, G. Morel, A. Micaelli, B. Cagneau, D. Bellot, On the force control of kinematically defective manipulators interacting with an unknown environment, Control Systems Technology, IEEE Transactions on 18 (2) (2010) 307–322.

[3] N. Zemiti, T. Ortmaier, M.-A. Vitrani, G. Morel, A force controlled laparoscopic surgical robot without distal force sensing, in: ISER, 2004, pp. 153–164.

[4] M. Michelin, E. D. P. Poignet, Experimental study of dynamic task / posture decoupling in minimally invasive surgery motions., n proceeding of the 9th International Symposium on Experimental Robotics (ISER'04) (2004) 217–226.

[5] T. Haidegger, B. Benyó, L. Kovács, Z. Benyó, Force sensing and force control for surgical robots, Proc. of the 7th IFAC Symposium on Modeling and Control in Biomedical Systems (2009) 413–418.

[6] F. Pierrot, E. Dombre, E. Dégoulange, L. Urbain, P. Caron, J. Gariépy, J. Mégnien, Hippocrate: A safe robot arm for medical applications with force feedback, Medical Image Analysis 3 (1999) 285–300.

[7] E. Dombre, G. Duchemin, P. Poignet, F. Pierrot, Dermarob: A safe robot for recontructive surgery, IEEE Transactions on Robotics 19 (2003) 876–884.

[8] J. M. Florez, J. Szewczyk, G. Morel, An impedance control strategy for a hand-held instrument to compensate for physiological motion, In Proc. IEEE International Conference on Robotics and Automation (ICRA) (2012) 1952–1957.

[9] L. A. Sánchez, M. Q. Le, C. Liu, N. Zemiti, P. Poignet, The impact of interaction model on stability and transparency in bilateral teleoperation for medical applications, In Proc. IEEE International Conference on Robotics and Automation (ICRA) (2012) 1607–1613.

[10] O. Khatib, J. Burdick, Motion and force control of robot manipulators, In Proc. IEEE International Conference on Robotics and Automation (ICRA) (1986) 1381–1386.

[11] P. Moreira, C. Liu, N. Zemiti, P. Poignet, Beating heart motion compensation using active observers and disturbance estimation, In Proc. IFAC Symposium on Robot Control.

[12] C. Liu, P. Moreira, N. Zemiti, P. Poignet, 3d force control for robotic-assisted beating heart surgery based on viscoelastic tissue model, In Proc. Annual International Conference of the IEEE Engineering in Medicine and Biology Society (EMBC) (2011) 7054–7058.

[13] R. Cortesão, R. Koeppe, U. Nunes, G. Hirzinger, Explicit force control for manipulators with active observers, In Proc. IEEE International Conference on Intelligent Robots and Systems (IROS).

[14] P. Moreira, C. Liu, N. Zemiti, P. Poignet, Soft tissue force control using active observers and viscoelastic interaction model, In Proc. IEEE International Conference on Robotics and Automation (ICRA) (2012) 4660–4666.

[15] Y. Kobayashi, P. Moreira, C. Liu, N. Zemiti, P. Poignet, M. Fujie, Haptic feedback control in medical robots through fractional viscoelastic tissue model, In Proc. Annual International Conference of the IEEE Engineering in Medicine and Biology Society (EMBC) 36 (2011) 6704–6708.

[16] K. J. Aström, B. Wittenmark, Computer-Controlled Systems: Theory and Design, 3rd Edition, Prentice Hall, 1996.

[17] M. Cespi, G. Bonacucina, M. Misici-Falzi, R. Golzi, L. Boltri, G. F. Palmieri, Stress relaxation test for the characterization of the viscoelasticity of pellets, European Journal of Pharmaceutics and Biopharmaceutics 67 (2007) 476–484.

[18] P. Jordana, S. Socrateb, T. E. Zicklera, R. D. Howe, Constitutive modeling of porcine liver in indentation using 3d ultrasound imaging, Journal of the Mechanical Behavior of Biomedical Materials 2 (2009) 192–201.

[19] M. Marchal, Modélisation des tissus mous dans leur environnement pour l'aide aux gestes médico-chirurgicaux, Ph.D. thesis, University Joseph Fourier (2006).
[20] R. Cortesão, On kalman active observers, Journal of Intelligent and Robotic Systems 48 (2007) 131–155.
[21] R. Cortesão, W. Zarrad, P. Poignet, O. Company, E. Dombre, Haptic control design for robotic-assisted minimally invasive surgery, In Proc. IEEE International Conference on Intelligent Robots and Systems (IROS) 285 (2006) 454–459.
[22] H. Paul, W. Bargar, B. Mittelstadt, B. Musits, R. Taylor, P. Kazanzides, Development of a surgical robot for cementless total hip arthroplasty, Clinical Orthopaedics and Related Research 285 (1992) 57–66.
[23] F. L. Lewis, Applied optimal control & estimation: digital design & implementation, Prentice Hall, Englewood Cliffs, New Jersey, USA, 1992.
[24] T. Yamamoto, Applying tissue models in teleoperated robot-assisted surgery, Ph.D. thesis, The Johns Hopkins University (2011).
[25] N. Diolaiti, C. Melchiorri, Contact impedance estimation for robotic systems, IEEE Transactions on Robotics 21 (5) (2005) 925–935.
[26] C. Chui, E. Kobayashi, X. Chen, T. Hisada, I. Sakuma, Combined compression and elongation experiments and non-linear modelling of liver tissue for surgical simulation, Medical & biological engineering & computing 42 (6) (2004) 787–98.
[27] Z. Gao, K. Lister, J. Desai, Constitutive modeling of liver tissue: experiment and theory., Annals of Biomedical Engineering 38 (2) (2010) 505–516.
[28] Y. Kobayashi, A. Kato, H. Watanabe, T. Hoshi, K. Kawamura, M. G. Fujie, Modeling of viscoelastic and nonlinear material properties of liver tissue using fractional calculations, Journal of Biomechanical Science and Engineering 7 (2) (2012) 177–187.
[29] T. Yamamoto, B. Vagvolgyi, K. Balaji, L. L. Whitcomb, A. M. Okamura, Tissue property estimation and graphical display for teleoperated robot-assisted surgery, In Proc. IEEE International Conference on Robotics and Automation (ICRA) (2009) 4239–4245.
[30] K. Hunt, F. Crossley, Coefficient of restitution interpreted as damping in vibroimpact, ASME Journal of Applied Mechanics 42 (1975) 440–445.
[31] S. Bhasin, K. Dupree, P. M. Patre, W. E. Dixon, Neural network control of a robot interacting with an uncertain hunt-crossley viscoelastic environment, ASME Dynamic Systems and Control Conference (2008) 875–882.
[32] L. Barbé, B. Bayle, M. de Mathelin, In vivo model estimation and hapatic chacterization of needle insertions, The Int. Journal of Robotics Research 26 (2007) 1283–1301.
[33] A. M. Okamura, L. N. Verner, C. E. Reiley, M. Mahvash, Haptics for robot-assisted minimally invasive surgery, 13th International Symposium of Robotics Research (2007) 26–29.
[34] H. Delingette, Towards realistic soft tissue modeling in medical simulation, Projet Epidaure - Rappotde recherche n3506.
[35] M. Dominici, P. Poignet, E. Dombre, Compensation of physiological motion using linear predictive force control, In Proc. IEEE International Conference on Intelligent Robots and Systems (IROS) (2008) 1173–1178.
[36] M. Dominici, R. Cortesão, C. Sousa, Heart motion compensation for robotic-assisted surgery predictive approach vs. active observer, In Proc. IEEE International Conference on Robotics and Automation (ICRA) (2011) 6252–6257.
[37] B. Cagneau, N. Zemiti, D. Bellot, G. Morel, Physiological motion compensation in robotized surgery using force feedback control, In Proc. IEEE International Conference on Robotics and Automation (ICRA) (2007) 1881–1886.
[38] Z. Zarrouk, A. Chemori, P. Poignet, Adaptive force feedback control for 3d compensation of physiological motion in beating heart surgery, In Proc. IEEE International Conference on Intelligent Robots and Systems (IROS) (2010) 1856–1861.
[39] Y. C. Fung, Biomechanics: Mechanical Properties of Living Tissue, Springer, 1993.
[40] Y. Kobayashi, A. Onishi, H. Watanabe, T. Hoshi, K. Kawamura, M. G. Fujie, In vitro validation of viscoelastic and nonlinear physical model of liver for needle insertion simulation, Int. Conf. on Biomedical Robotics and Biomachatronics (2008) 469–476.
[41] R. Cortesão, On kalman active observers, Journal of Intelligent and Robotic Systems 48 (2007) 131–155.
[42] L. Sciavicco, B. Siciliano, Modeling and Control of Robot Manipulators, Springer, 2000.
[43] K. B. Reed, A. M. Okamura, N. J. Cowan, Modeling and control of needles with torsional friction., IEEE Transactions on Biomedical Engineering 56 (12) (2009) 2905–2916.
[44] S. Misra, K. B. Reed, B. W. Schafer, K. T. Ramesh, A. M. Okamura, Mechanics of flexible needles robotically steered through soft tissue, The International Journal of Robotics Research 29 (13) (2010) 1640–1660.
[45] V. Kallem, N. Cowan, Image guidance of flexible tip-steerable needles, IEEE Transactions on Robotics 25 (1) (2009) 191–196.